

Article

Numerical Investigation on the Effect of Wet Steam and Ideal Gas Models for Steam Ejector Driven by Ship Waste Heat

Nan He [†], Xiaolong Chi [†], Chi Feng, Manfei Lu, Li Zhang and Jingming Dong ^{*†} 

Marine Engineering College, Dalian Maritime University, Dalian 116026, China; hexiaonan@dmlu.edu.cn (N.H.); m15504090161@163.com (X.C.); fc11@dmlu.edu.cn (C.F.); lumanfei1120221216@dmlu.edu.cn (M.L.); 0816zl@dmlu.edu.cn (L.Z.)

* Correspondence: dmudjm@dmlu.edu.cn

[†] These authors contributed equally to this work.

Abstract: Steam ejectors could improve the energy efficiency of ships by efficiently utilizing low-grade waste heat from ships for seawater desalination or cooling. The internal flow characteristics of steam ejectors can be deeply analyzed through numerical simulation, which is of great significance for improving their performance. Due to the influence of the nonequilibrium phase change, the results of the wet steam model and the ideal gas model are significantly different. In this paper, the flow field characteristics of the wet steam model and the ideal gas model under different primary flow pressures (P_m) are compared and analyzed. The results show that the structures of the shock wave train for the wet steam model and the ideal gas model are different under different P_m . When the first shock wave of the shock wave train changes from a compression shock wave to an expansion shock wave, the P_m for the ideal gas model is 75,000 Pa and that for the wet steam model is 55,000 Pa. The phase change reduces the energy loss of the shock wave. With the increase in the P_m , the variation in the length of the shock wave train for the wet steam model decreases by 61%, the variation of the primary temperature at the nozzle exit increases by 60% and the variation in the choke temperature decreases by 50% compared with the ideal gas model. The investigation in this paper provides guidance for the design theory of a ship waste heat steam ejector.



Citation: He, N.; Chi, X.; Feng, C.; Lu, M.; Zhang, L.; Dong, J. Numerical Investigation on the Effect of Wet Steam and Ideal Gas Models for Steam Ejector Driven by Ship Waste Heat. *Appl. Sci.* **2023**, *13*, 12516. <https://doi.org/10.3390/app132212516>

Academic Editor: José A. Orosa

Received: 9 October 2023

Revised: 11 November 2023

Accepted: 14 November 2023

Published: 20 November 2023



Copyright: © 2023 by the authors. Licensee MDPI, Basel, Switzerland. This article is an open access article distributed under the terms and conditions of the Creative Commons Attribution (CC BY) license (<https://creativecommons.org/licenses/by/4.0/>).

Keywords: ship energy saving; steam ejector; non-equilibrium phase change; wet steam model; ideal gas model

1. Introduction

Under the trend of global warming, countries are striving to achieve the target carbon peak [1]. The energy consumption of the shipping industry is huge, and ship energy saving and emission reduction have become hot issues. A large amount of low-grade waste heat is generated during a voyage, such as waste heat from the jacket water and exhaust gas of the main engine. The rational utilization of waste heat could effectively improve the energy efficiency of ships and reduce carbon emissions. Due to its advantages in energy saving and emission reduction [2], the steam ejector is widely used in low-grade energy utilization systems, such as low-temperature multieffect distillation [3] and waste heat refrigeration [4]. Therefore, it is of great significance to investigate steam ejectors driven by ship waste heat.

The primary flow pressure (P_m) or primary flow temperature (T_m) have an important effect on the performance of the steam ejector. Sun et al. [5] studied the influence of the T_m on the performance of a steam ejector in a refrigeration system. The results showed that the entrainment ratio increased first and then decreased when the temperature rose. Additionally, there was an optimal T_m . Sriveerakul et al. [6] found that the critical back pressure of the steam ejector increased with an increase in the T_m . Dong et al. [7,8] found that steam ejectors could be driven with heat sources at temperatures lower than 80 °C in a

refrigeration system and a single-effect thermal vapor compression desalination system. The entrainment ratio of the steam ejector could be increased effectively by decreasing the P_m and increasing the secondary flow pressure (P_e).

There are complex flow phenomena in steam ejectors, such as the shock wave and choked flow. The numerical simulation method can be used to deeply analyze the complex flow characteristics inside steam ejectors, which would be of great value in improving their performance [9]. Dong et al. [10] adopted the ideal gas model to carry out numerical simulations on a steam ejector. They found that a series of diamond-shaped shock waves formed at the nozzle exit. Wang et al. [11] studied the influence of the P_m on the shock wave train and the choking effect. It was found that the length of the shock wave train increased, the position of the shock choke moved downstream and the choking effect increased with the increase in the P_m . Varga et al. [12] found that the P_m would not affect the nozzle efficiency and entrainment ratio when the steam ejector was in a critical state. Pianthong et al. [13] found that the width of the shock wave train increased when the P_m increased. This reduced the flow area of the secondary flow and, thus, reduced the entrainment ratio. Li et al. [14] found that the change in the P_m resulted in three states of fluid at the nozzle exit: underexpansion, complete expansion and overexpansion. When the state of the fluid changed from underexpansion to overexpansion, the entropy generation inside the ejector increased.

The physical properties and phase change of working fluid have a significant influence on simulation results. Wang et al. [15] considered the condensation inside a steam ejector for a simulation. They found that the critical back pressure calculated with the wet steam model was slightly lower than that calculated with the ideal gas model. Sharifi [16] and Zheng [17] proposed that the critical back pressure and entrainment ratio predicted with the wet steam model were both higher than those predicted with the ideal gas model. Foroozesh et al. [18] compared the entrainment ratio calculated with the wet steam model and the ideal gas model with the experimental results. The comparison results showed that the results calculated with the wet steam model were closer to the experimental results. Ariaifar et al. [19] compared and analyzed the thickness of the mixed layer between the primary flow and the secondary flow in a steam ejector calculated with the wet steam model and the ideal gas model. They also explained why the ejection ratio calculated with the wet vapor model was higher than that calculated with the ideal gas model. Lei et al. [20] employed the wet steam model to optimize the steam ejector's geometry. Compared to the ideal gas model, the use of the wet steam model dramatically decreased the entrainment ratio error from 16.24% for single-phase steam to 3.92% when compared to experimental data. Wang et al. [21] analyzed in detail the condensation process inside steam ejectors. They found that the most intensive condensation happened at the primary nozzle downstream and nozzle exit region. Zhang et al. [22,23] modified the nonequilibrium condensation model. The results showed that the modified model could describe the flow characteristics inside the steam ejector more accurately. Therefore, an accurate calculation of the flow characteristics inside the steam ejector was found to be key to improving its performance. However, most current studies have assumed steam as an ideal gas and ignored the effects of the nonequilibrium phase change. This has resulted in a large deviation between simulation results and the actual phenomenon [24]. Moreover, the effect of the nonequilibrium phase change on the characteristics inside the steam ejector is also lacking.

In this paper, a wet steam model considering the nonequilibrium phase change is established to analyze the flow characteristics inside a steam ejector. The effects of the wet steam model and the ideal gas model on the pressure distribution, temperature distribution and Mach number distribution inside the steam ejector under different P_m are compared and analyzed. At the same time, the influence of the phase change on the flow characteristics of the steam ejector is explained through the distribution of the supercooling degree and wetness fraction.

2. Mathematical Modelling and CFD Modelling

2.1. Mathematical Modelling

In this paper, the governing equations of the vapor–liquid two-phase flow were described using the Eulerian–Eulerian model, and the following assumptions were considered when establishing the model.

- (1) The flow of fluid was considered to be compressible, adiabatic and continuous in the flow field.
- (2) The nucleation of the steam was spontaneous nucleation without the influence of external condensation nuclei.
- (3) The generated droplets were very small and incompressible spheres. Regardless of the slip flow between the vapor–liquid phases, the droplets were uniformly dispersed in the vapor phase.
- (4) There was no collision or polymerization between droplets or between droplets and the walls.

Based on the above assumptions, the vapor-phase flow governing the equations of the wet steam model were as follows:

$$\frac{\partial \rho}{\partial t} + \frac{\partial(\rho u_j)}{\partial x_j} = -\dot{m}, \tag{1}$$

$$\frac{\partial}{\partial t}(\rho u_i) + \frac{\partial}{\partial x_j}(\rho u_i u_j) = -\frac{\partial p}{\partial x_i} + \frac{\partial \tau_{ij}}{\partial x_j} - u \dot{m}, \tag{2}$$

$$\frac{\partial}{\partial t}(\rho E) + \frac{\partial}{\partial x_j}(u_j(\rho E + p)) = -\frac{\partial}{\partial x_j}(\lambda_{eff} \frac{\partial T}{\partial x_j}) + \frac{\partial}{\partial x_j}(u_i \tau_{ij}) + h_{lt} \dot{m}, \tag{3}$$

where ρ is the density, u is the velocity, p is the pressure, h_{lt} is the latent heat of vaporization and E is the total enthalpy.

The liquid-phase condensation control equation included the liquid-phase mass fraction equation and the liquid drop number equation [25], and were as follows:

$$\frac{\partial(\rho Y)}{\partial t} + \frac{\partial(\rho Y u_j)}{\partial x_j} = \dot{m}, \tag{4}$$

$$\frac{\partial(\rho N)}{\partial t} + \frac{\partial(\rho N u_j)}{\partial x_j} = \rho J, \tag{5}$$

where Y is the mass fraction of the liquid phase, N is the number of droplets, \dot{m} is the mass generation rate of the liquid phase and J is the nucleation rate.

The nucleation rate adopted the classical nucleation theory modified by Kantrowitz [26]:

$$J = \frac{q_c}{1 + \phi} \left(\frac{\rho_v^2}{\rho_l}\right) \sqrt{\frac{2\sigma}{M_{mole}\pi}} \exp^{-\left(\frac{4\pi r^*2\sigma}{3k_B T_v}\right)}, \tag{6}$$

where k_B is the Boltzmann constant, σ is the droplet surface tension and ϕ is the correction coefficient. Additionally, the correction coefficient [27] was as follows:

$$\phi = \left[1 + 2\frac{\gamma - 1}{\gamma + 1} \frac{h_{lv}}{RT_V} \left(\frac{h_{lv}}{RT_V} - \frac{1}{2}\right)\right]^{-1}, \tag{7}$$

In Equation (6), the droplet surface tension had an important effect on the nucleation rate. The droplet surface tension was calculated by adopting Benson’s modified surface tension model [28].

$$\sigma = \sigma_p \left(1 - \frac{\sqrt[3]{\rho_l/m}}{4.836r}\right), \tag{8}$$

$$\sigma_p = 235.8 \left(1 - \frac{T_d}{647.3}\right)^{1.256} \left[1 - 0.625 \left(1 - \frac{T_d}{647.3}\right)\right], \quad (9)$$

The mass generation rate of the liquid phase was as follows:

$$\dot{m} = \frac{4\pi r^{*3}}{3} \rho_l J + 4\pi \rho_l n r^2 \frac{dr}{dt}, \quad (10)$$

where r^* is the critical radius of the droplet, ρ_l is the density of the liquid phase, r is the droplet radius and $\frac{dr}{dt}$ is the droplet growth rate.

Based on the energy conservation equation proposed by Hill [29], the droplet growth rate equation was obtained as follows:

$$\frac{dr}{dt} = \frac{p}{h_{lv} \rho_l \sqrt{2\pi RT_v}} \frac{\gamma + 1}{2\gamma} C_p (T_d - T_v) \quad (11)$$

The physical properties of the steam, such as the enthalpy, entropy, viscosity and specific heat capacity at constant pressure, were calculated using empirical functions based on the second and third virial coefficients proposed by Young [30].

2.2. CFD Modelling

The steam ejector was mainly composed of four parts: the nozzle, mixing chamber, constant section and diffuser. The schematic diagram of the steam ejector is shown in Figure 1 and the structure parameters of the steam ejector are listed in Table 1 [31].

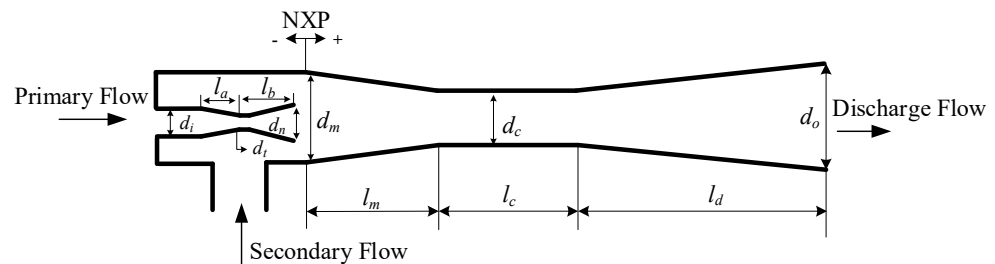


Figure 1. Schematic diagram of the steam ejector.

Table 1. Structure parameters of the steam ejector [31].

| Parameter Description | Symbol | Value | Units |
|----------------------------------|--------|--------|-------|
| Diameter of nozzle inlet | d_i | 34.51 | mm |
| Diameter of nozzle throat | d_t | 8.00 | mm |
| Diameter of nozzle outlet | d_n | 13.60 | mm |
| Converging length of nozzle | l_a | 75.06 | mm |
| Diverging length of nozzle | l_b | 49.66 | mm |
| Nozzle exit position | NXP | 0.00 | mm |
| Diameter of mixing chamber inlet | d_m | 36.55 | mm |
| Diameter of constant section | d_c | 25.40 | mm |
| Diameter of diffuser outlet | d_o | 53.69 | mm |
| Length of mixing chamber | l_m | 149.00 | mm |
| Length of constant section | l_c | 75.00 | mm |
| Length of diffuser | l_d | 209.65 | mm |

Since the steam ejector had an axisymmetric structure, the two-dimensional axisymmetric mesh could be used to replace the three-dimensional mesh [13]. ICEM was used to mesh the steam ejector. The mesh distribution of the steam ejector is shown in Figure 2. The meshes near the nozzle and the wall of the steam ejector were refined. Four meshes were selected for the grid independence verification analysis with a mesh number between 30,000 and 90,000. When the mesh number exceeded 78,000, the numerical simulation

results no longer changed. In order to save calculation time, it was determined that the mesh number of the steam ejector should be no less than 78,000.

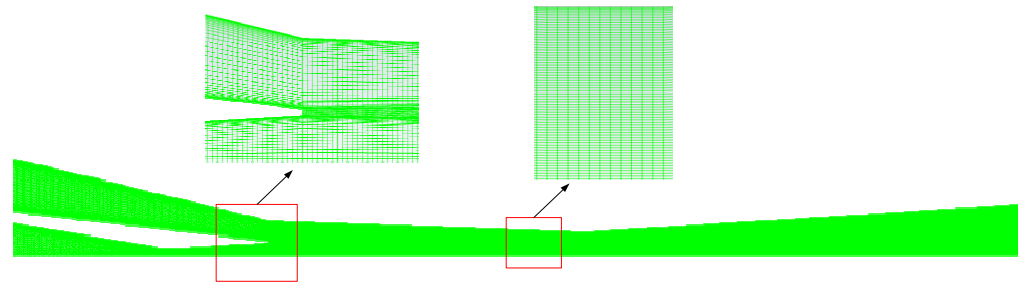


Figure 2. Mesh distribution.

In this paper, the finite volume method was used to solve the flow control equation, and the second-order upwind scheme was used to discretize the control equation. The coupled method was selected for the iterative solution. The liquid-phase control equation was compiled into UDF using C code and then added to FLUENT for the calculation. Condensation parameters, such as the nucleation rate and liquid mass formation rate, were calculated and stored in UDM. The relaxation factors for UDS 1 and UDS 2 were 0.8 and 0.4, respectively. The $k-\epsilon$ realizable turbulence model [18] was used to simulate the complex flow phenomena inside the steam ejector more accurately. The wall condition was set as a nonslip adiabatic wall. All residual values of the calculated results were less than 10^{-6} . The inlet and outlet of the steam ejector were set as the pressure inlet and pressure outlet, respectively. The specific values are shown in Table 2.

Table 2. Boundary conditions.

| P_m (Pa) | T_m (K) | P_e (Pa) | P_b (Pa) |
|---------------|-----------|------------|------------|
| 50,000–80,000 | 355–367 | 5000 | 6000 |

In order to verify the accuracy of the wet steam model, the experimental data obtained by Moore [32] and AL-Doori [33] were used in this paper to verify the calculation results of the model, as shown in Figure 3. It can be seen from the figures that the calculated results of the wet steam model were in good agreement with the experimental values. This indicated that the wet steam model established in this paper could not only accurately describe the nonequilibrium phase change process of the wet steam in the nozzle, but also accurately calculate the internal flow characteristic inside the steam ejector.

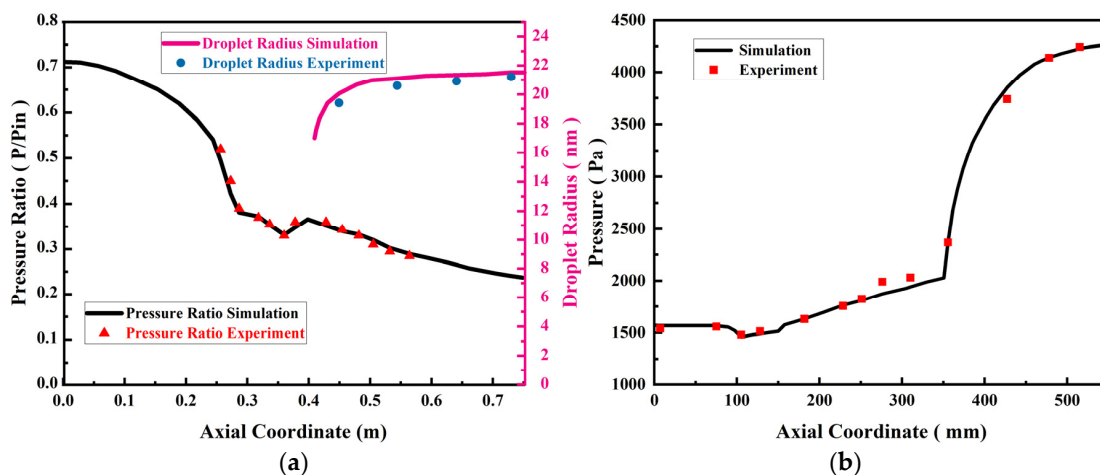


Figure 3. Comparison between experimental and numerical results. (a) Moore’s nozzle B; (b) steam ejector.

3. Results and Discussion

3.1. Nonequilibrium Phase Change Characteristics in Steam Ejectors

The nonequilibrium phase change process in the steam ejector was analyzed through the distribution of the steam subcooled degree and steam wetness fraction on the axis of the steam ejector. The subcooled degree is defined as the difference between the steam pressure and the saturation temperature. The distribution of the subcooled degree can reflect the variation trend of the steam thermodynamic state well. Figure 4 shows the distribution of the subcooled degree of the steam ejector axis under different P_m . It can be seen from the figure that the subcooled degree increased continuously after the primary flow passed through the nozzle throat. The droplet released latent heat of condensation in the process of growth based on condensation nuclei and the primary flow suddenly dropped. The inflection point of the subcooled degree is called the Wilson point [34]. When the primary flow passed through the nozzle outlet, a series of shock waves alternating between compression waves and expansion shock waves were generated in the mixing chamber. When the primary flow passed through the compression shock wave, the subcooled degree was negative; that is, the primary flow was in a superheated state. When the primary flow passed through the expansion shock wave, the subcooled degree increased further and the steam was in the nonequilibrium state of supercooling. When the primary flow was mixed with the secondary flow, a choking effect occurred in the mixing chamber. At this time, the subcooled degree of the primary flow reduced from 3 K to -18 K. This meant that the choking effect caused the mixed flow to overheat. After entering the diffuser, the mixed flow accelerated the expansion and the subcooled degree increased. Then, under the choking effect of the shock waves in the diffuser, the subcooled degree changed from positive to negative and the mixed flow changed from the supercooled state to the superheated state.

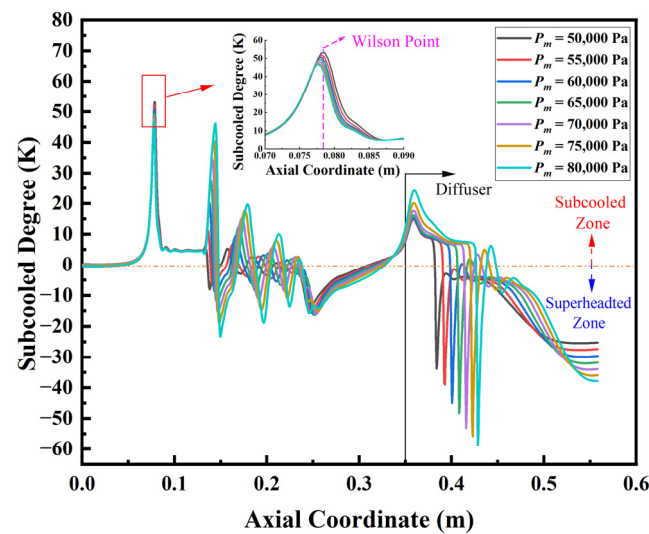


Figure 4. Subcooled degree distribution along the steam ejector axis under different P_m .

The distribution of the wetness fraction can reflect the process of the phase change in the steam ejector. A decrease in the wetness fraction means the droplet evaporates, while a rise in the wetness fraction means the droplet condenses. The distribution of the wetness fraction along the steam ejector axis under different P_m is shown in Figure 5. It can be seen from the figure that the wetness fraction increased rapidly at the Wilson point in the nozzle, while the wetness fraction decreased when the primary flow passed through the compression shock wave in the mixing chamber and increased when it passed through the expansion shock wave. According to the analysis in Figure 4, when the primary flow was in an overheated state in the compression shock wave, the droplet absorbed the heat and evaporated, resulting in a decrease in the wetness fraction. In addition, when the primary flow was in a supercooled nonequilibrium state in the expansion shock wave, the

droplets continued to condense and release the latent heat of the condensation, resulting in an increase in the wetness fraction. The mixed flow continued to expand after entering the diffuser and the condensation of the droplets increased the wetness fraction. After the mixed flow passed through the shock wave, a large number of droplets evaporated and the wetness fraction dropped sharply until it reached zero.

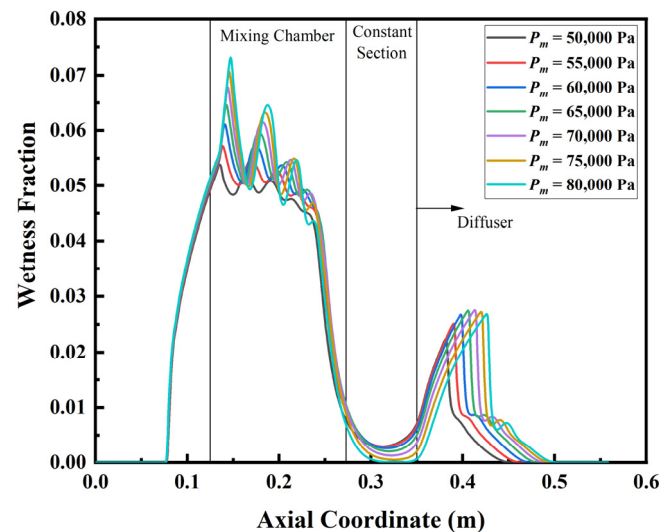


Figure 5. Wetness fraction distribution along the steam ejector axis under different P_m .

3.2. Comparative Analysis of Internal Flow Characteristics Inside Steam Ejectors

Compared with the ideal gas model, the nonequilibrium phase change of steam was considered in the wet steam model. Therefore, the difference in pressure, temperature and Mach number distribution between the wet steam model and the ideal gas model under different P_m was compared and analyzed in this paper.

The shock wave was formed in the mixing chamber after the high-temperature and high-pressure primary flow accelerated through the Laval nozzle, which caused the pressure of the primary flow to change dramatically. Therefore, the distribution of pressure could reflect the characteristics of the shock wave well. Figure 6 shows the pressure contours of the steam ejector for the wet steam model and the ideal gas model under different P_m . By comparing the two figures, it could be seen that the shape of the shock wave train changed when the P_m increased. The first shock wave of the shock wave train changed from the compression shock wave to the expansion shock wave. For the wet steam model, the first shock wave changed from the compression shock wave to the expansion shock wave when the P_m was 55,000 Pa. For the ideal gas model, the compression shock wave changed to the expansion shock wave when the P_m was 75,000 Pa. The P_m for the wet steam model was significantly lower than that for the ideal gas model, by 27%. In addition, the number of shock wave trains for the wet steam model was seven, while the number of shock wave trains for the ideal gas model was nine. With the increase in the P_m , the length of the shock wave train in the mixing chamber increased. Comparing the results of the wet steam model and the ideal gas model, it was found that the change in the shock wave train length of the wet steam model was shorter than that of the ideal gas model.

The pressure at the nozzle exit had an important effect on the shape of the shock wave train in the mixing chamber. When the pressure at the nozzle exit was lower than the mixing chamber pressure, the primary flow was in a state of overexpansion, resulting in an expansion shock wave. When the pressure at the nozzle exit was higher than the mixing chamber pressure, the primary flow was in the underexpansion state, resulting in an expansion shock wave. In order to quantitatively analyze the difference in the pressure at the nozzle exit between the two models, the pressure distribution along the steam ejector axis under different P_m is shown in Figure 7. It was found that the pressure at the nozzle

exit for the wet steam model was 5320 Pa and the pressure at the nozzle exit for the ideal gas model was 3933 Pa, while the P_m was 50,000 Pa. The pressure at the nozzle exit for the wet steam model was 35.2% higher than that for the ideal gas model. According to the analysis of the nonequilibrium phase change characteristics, it could be seen that the primary flow was in the supercooled nonequilibrium state during the expansion in the nozzle, and a large number of condensation nuclei formed at this time. The droplets grew and released latent heat of condensation, which caused the P_m to rise. Therefore, there were differences in the shape of the shock wave train between the wet steam model and the ideal gas model under different P_m .

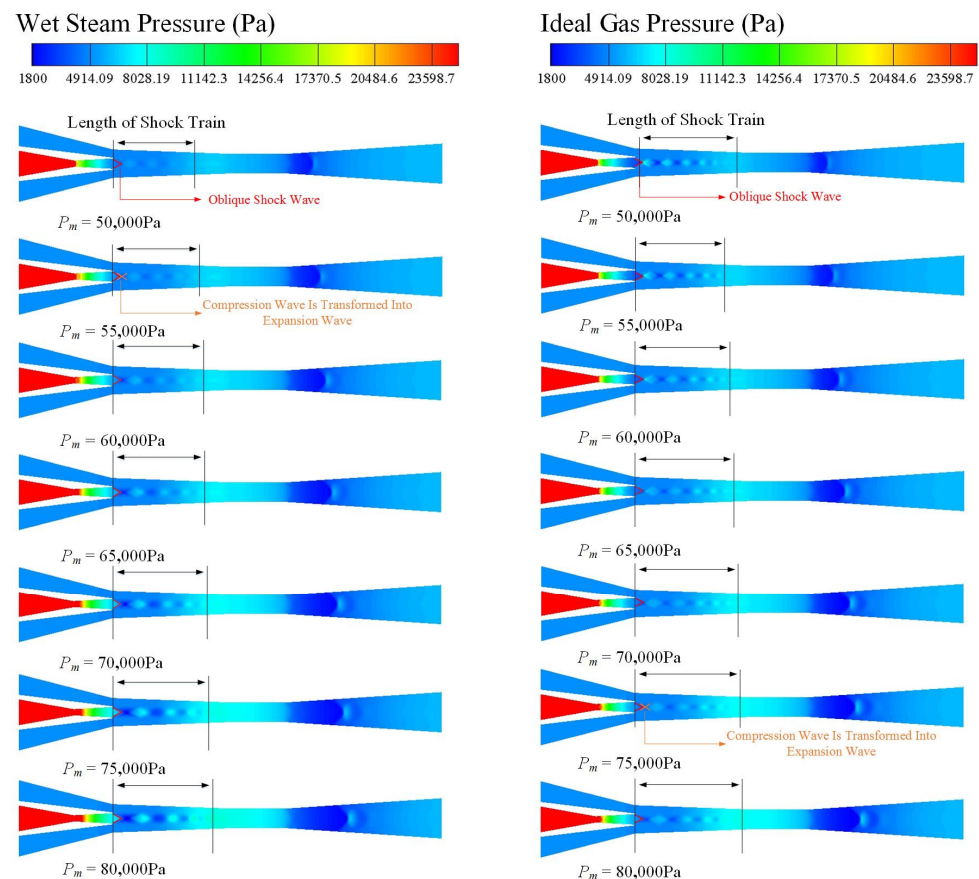


Figure 6. Pressure contours under different P_m for wet steam model and ideal gas model.

Compared with the ideal gas model, the condensation phase change was also considered in the wet vapor model. The latent heat of condensation released by the condensation phase change process caused the temperature field inside the steam ejector calculated with the two models to be very different. The temperature distribution for the wet steam model and the ideal gas model under different P_m is shown in Figure 8. It can be seen from the figure that the temperature in the nozzle divergence section for the wet steam model was significantly higher than that for the ideal gas model. In addition, the average temperature of the shock wave train in the mixing chamber for the wet steam model was also higher than that for the ideal gas model. This was due to the nonequilibrium condensation phenomenon in the expansion process of the primary flow and the release of latent heat of condensation.

In order to further analyze the difference in the temperature distribution between the two models, the temperature distribution along the steam ejector axis under different P_m is shown in Figure 9. It can be seen that when the P_m was 50,000 Pa, the temperature at the nozzle exit for the wet steam model was 315 K, and that for the ideal gas model was 183 K. The temperature at the nozzle exit for the wet steam model was 72.1% higher than

that for the ideal gas model. With the increase in P_m , the temperature at the nozzle exit increased from 315 K to 324 K for the wet steam model and the temperature at the nozzle exit increased from 183 K to 188 K for the ideal gas model. According to the analysis of the nonequilibrium phase change characteristics, it could be seen that the Wilson point moved towards the nozzle throat and the condensation position was closer to the nozzle throat with the increase in the P_m . This increased the amount of condensation in the liquid phase of the nozzle divergence section and the release of latent heat. Therefore, the change in the temperature at the nozzle exit for the wet steam model was larger than that for the ideal gas model. The choking effect occurred near the inlet of the constant section. When the P_m was 50,000 Pa, the choking temperature for the wet steam model was 325 K, and that for the ideal gas model was 336 K. In the process of mixing the primary flow and the secondary flow, the mixed flow was in the superheated state. At this time, the liquid-phase evaporation absorbed the heat of the surrounding mixed flow and reduced its temperature. Therefore, the choking temperature for the wet steam model was lower than that for the ideal gas model. With the increase in the P_m , the choking temperature for the wet steam model increased from 325 K to 329 K and the choking temperature for the ideal gas model increased from 336 K to 342 K. After the mixed flow entered the diffuser, the temperature decreased due to expansion. Then, the temperature rose suddenly because of the shock wave. With the increase in the P_m , the temperature before the shock wave in the diffuser decreased from 284 K to 282 K for the wet steam model and decreased from 250 K to 224 K for the ideal gas model. The mixed flow was supercooled during the expansion. When the subcooled degree reached a certain threshold, the droplets began to condense. The latent heat released during the condensation process caused the T_m to rise and was close to the saturated state. The increase in the P_m caused the expansion of the primary flow to increase and the T_m to decrease rapidly. However, at the same time, the amount of condensation in the liquid phase also increased. This allowed more latent heat of condensation to be released into the primary flow and, thus, offset the decrease in the T_m caused due to the expansion. Therefore, the variation in the T_m before the shock wave for the wet steam model was smaller than that for the ideal gas model.

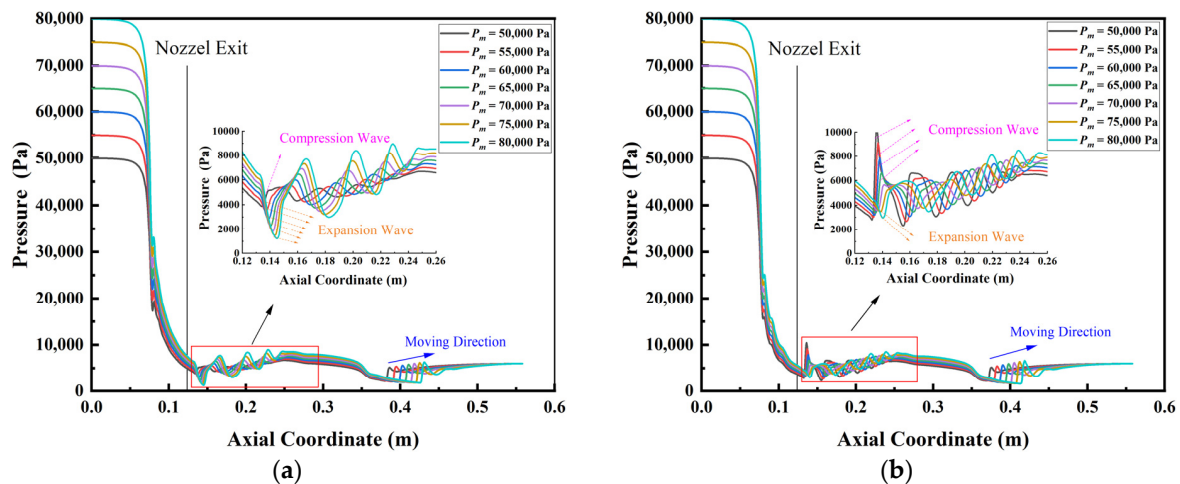


Figure 7. Pressure distribution along the steam ejector axis under different P_m . (a) Wet steam model; (b) ideal gas model.

The variation in the Mach number could reflect the shock wave intensity well. The Mach number contour for the wet steam model and the ideal gas model under different P_m is shown in Figure 10. It was found that the Mach number at the nozzle exit for the wet steam model was lower than that for the ideal gas model. Combined with the analysis of the pressure distribution, it could be seen that the release of condensation latent heat in the nozzle produced condensation shock waves in the nozzle divergence section. The choking effect of the condensation shock wave resulted in a decrease in the Mach number.

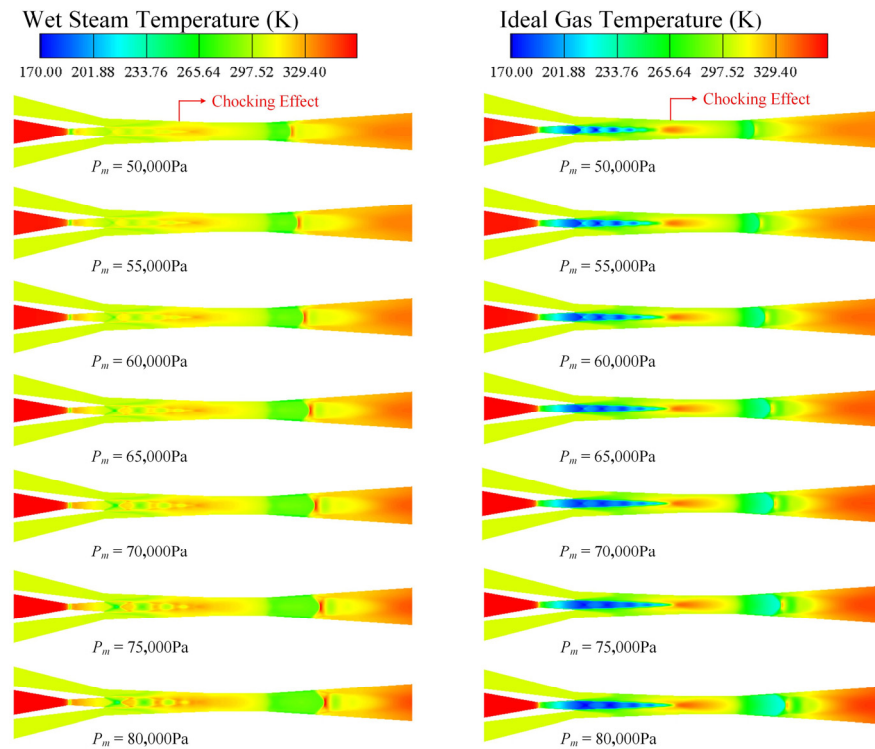


Figure 8. Temperature contours under different P_m for wet steam model and ideal gas model.

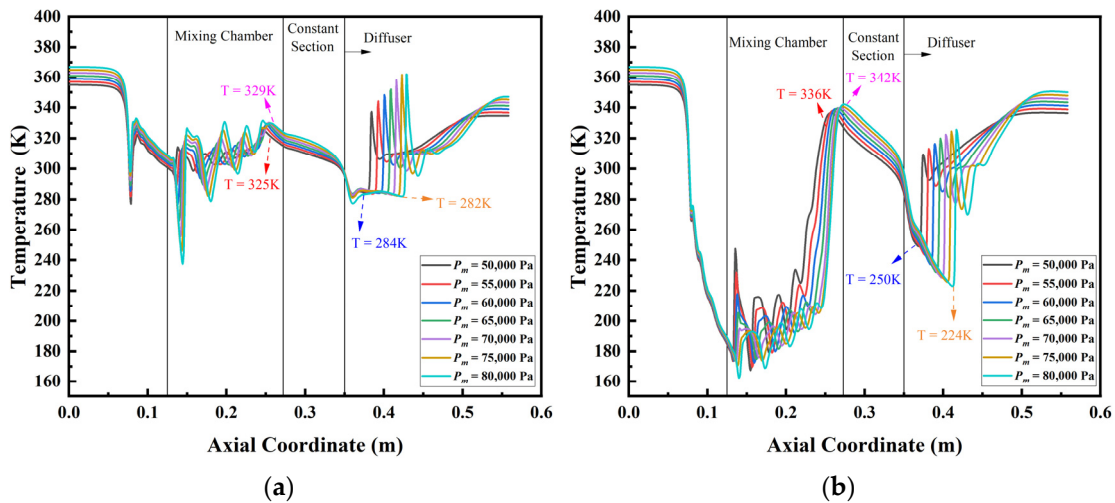


Figure 9. Temperature distribution along the steam ejector axis under different P_m . (a) Wet steam model; (b) ideal gas model.

The Mach number distribution under different P_m is shown in Figure 11. When the P_m was 50,000 Pa, the Mach number at the nozzle exit for the wet steam model was 2, and that for the ideal gas model was 2.37. When the P_m increased from 50,000 Pa to 80,000 Pa, the axial position at the end of the shock wave train for the wet steam model varied from 0.229 m to 0.237 m, and that for the ideal gas model varied from 0.231 m to 0.247 m. According to the analysis in Figure 4, it could be seen that the primary flow was in an overheated state when it passed through the compression shock wave, while it was in a supercooled state when it passed through the expansion shock wave. This caused the droplets to evaporate and condense continuously within the shock wave train. In this process, the condensation latent heat absorbed and released by the droplet caused the T_m and the P_m to slightly fluctuate, thus, reducing the energy loss of the shock wave. Therefore, the variation in the length of the shock wave train for the wet steam model was shorter

than that for the ideal gas model. In the diffuser, the mixed flow changed from a supersonic fluid to a subsonic fluid, and the Mach number suddenly decreased. When the P_m was 80,000 Pa, the Mach number for the wet steam model decreased from 1.78 to 0.78 and the Mach number for the ideal gas model decreased from 1.92 to 0.77. This showed that the variation range of the secondary shock wave in the diffuser for the wet steam model was smaller than that for the ideal gas model.

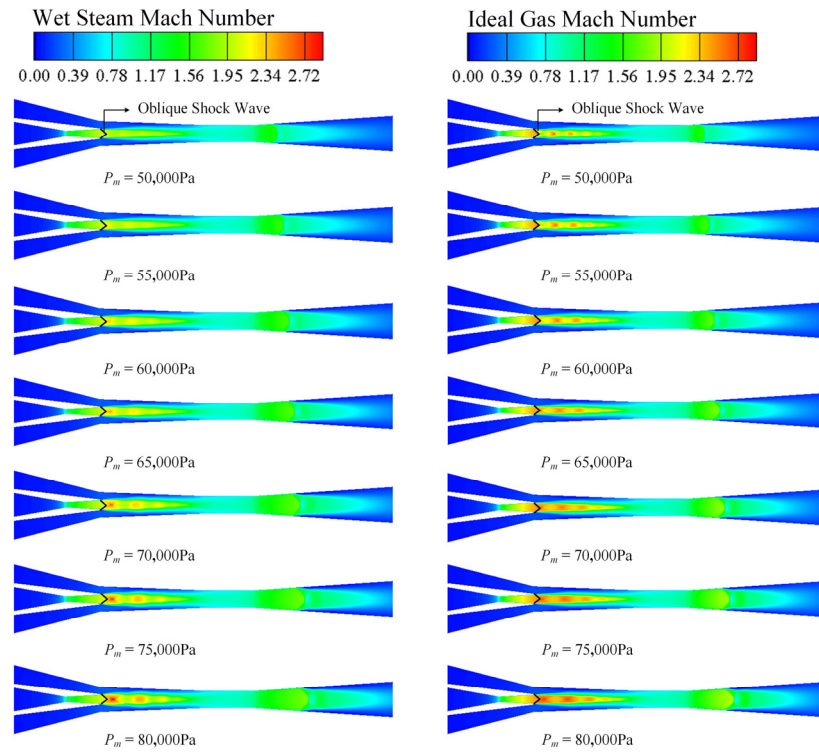


Figure 10. Mach number contour under different P_m for wet steam model and ideal gas model.

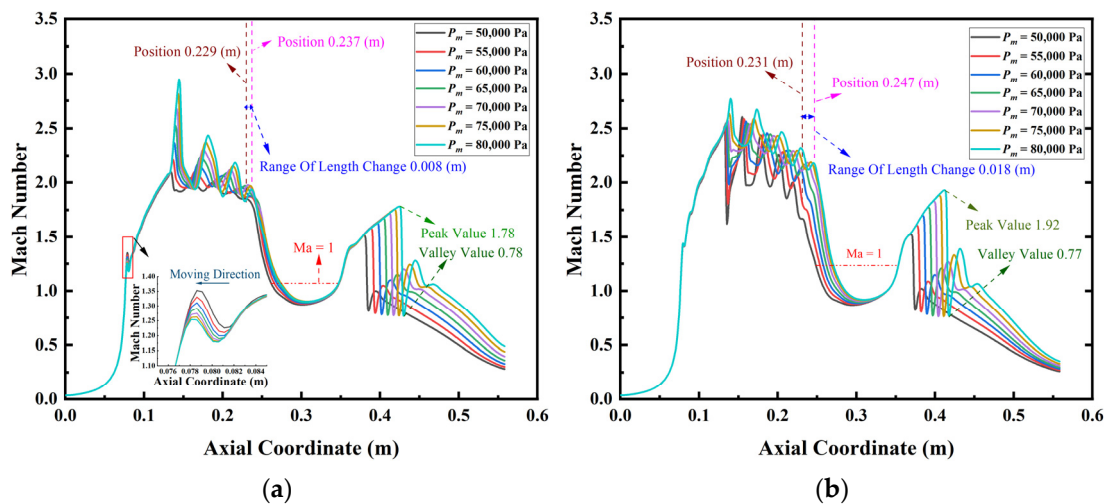


Figure 11. Mach number distribution along the steam ejector axis under different P_m . (a) Wet steam model; (b) ideal gas model.

4. Conclusions

To fully utilize the low-grade energy from ships and reduce carbon dioxide emissions, this paper established a wet steam model that considered the nonequilibrium phase change. The effect of the phase change on the internal flow of the steam ejector was studied and the

results for the wet steam model and the ideal gas model under different P_m were compared. The main conclusions were as follows:

- (1) Under different P_m , the structures of the shock wave train for the wet steam model and the ideal gas model were different. For the wet steam model, the first shock wave changed from a compression shock wave to an expansion shock wave when the P_m was 55,000 Pa. For the ideal gas model, the compression shock wave changed to an expansion shock wave when the P_m was 75,000 Pa.
- (2) When the P_m was 50,000 Pa, the primary temperature at the nozzle exit for the wet steam model increased by 72.1%, and the choke temperature at the constant section decreased by 3.4% compared with the ideal gas model. With the increase in the P_m , the variation in the primary temperature at the nozzle exit increased by 60%, the variation in the choke temperature decreased by 50% and the variation in the temperature before the shock wave in the diffuser decreased by 92.3%.
- (3) The phase change reduced the fluctuation of the P_m and the T_m , which reduced the energy loss of the shock wave. When the P_m increased from 50,000 Pa to 80,000 Pa, the variation in the length of the shock wave train for the wet steam model decreased by 61% compared with the ideal gas model.

In conclusion, there were significant differences between the wet steam model and the ideal gas model on the flow characteristics inside the steam ejector under different working conditions. The research in this paper provides a reference for the design theory of a ship's waste heat steam ejector. In future research, the influence of various models on the flow characteristics inside steam ejectors should be further studied, especially the real gas model.

Author Contributions: Validation, investigation, writing and editing, N.H. and X.C.; conceptualization, investigation, writing and editing, project administration and funding acquisition, J.D.; methodology and investigation, C.F., M.L. and L.Z. All authors have read and agreed to the published version of the manuscript.

Funding: This research was supported by the National Natural Science Foundation of China (grant no. 51979022).

Institutional Review Board Statement: Not applicable.

Informed Consent Statement: Not applicable.

Data Availability Statement: All data have been provided in the paper.

Conflicts of Interest: The authors declare no conflict of interest.

References

1. Zhang, G.; Dykas, S.; Li, P.; Li, H.; Wang, J. Accurate condensing steam flow modeling in the ejector of the solar-driven refrigeration system. *Energy* **2020**, *212*, 118690. [[CrossRef](#)]
2. Tashtoush, B.M.; Al-Nimr, M.A.; Khasawneh, M.A. A comprehensive review of ejector design, performance, and applications. *Appl. Energy* **2019**, *240*, 138–172. [[CrossRef](#)]
3. Han, B.; Liu, Z.; Wu, H.; Li, Y. Experimental study on a new method for improving the performance of thermal vapor compressors for multi-effect distillation desalination systems. *Desalination* **2014**, *344*, 391–395. [[CrossRef](#)]
4. Han, Y.; Sun, Y.; Wu, J. An efficient solar-aided waste heat recovery system based on steam ejector and WTA pre-drying in solar/lignite hybrid power plants. *Energy* **2020**, *208*, 118372. [[CrossRef](#)]
5. Sun, D. Experimental Investigation of the Performance Characteristics of a Steam Jet Refrigeration System. *Energy Sources* **1997**, *19*, 349–367. [[CrossRef](#)]
6. Sriveerakul, T.; Aphornratana, S.; Chunnanond, K. Performance prediction of steam ejector using computational fluid dynamics: Part 1. Validation of the CFD results. *Int. J. Therm. Sci.* **2007**, *46*, 812–822. [[CrossRef](#)]
7. Dong, J.; Wang, W.; Han, Z.; Ma, H.; Deng, Y.; Su, F.; Pan, X. Experimental Investigation of the Steam Ejector in a Single-Effect Thermal Vapor Compression Desalination System Driven by a Low-Temperature Heat Source. *Energies* **2018**, *11*, 2282. [[CrossRef](#)]
8. Dong, J.; Yu, M.; Wang, W.; Song, H.; Li, C.; Pan, X. Experimental investigation on low-temperature thermal energy driven steam ejector refrigeration system for cooling application. *Appl. Therm. Eng.* **2017**, *123*, 167–176. [[CrossRef](#)]
9. Ji, M.; Utomo, T.; Woo, J.; Lee, Y.; Jeong, H.; Chung, H. CFD investigation on the flow structure inside thermo vapor compressor. *Energy* **2010**, *35*, 2694–2702. [[CrossRef](#)]

10. Dong, J.; Hu, Q.; Yu, M.; Han, Z.; Cui, W.; Liang, D.; Ma, H.; Pan, X. Numerical investigation on the influence of mixing chamber length on steam ejector performance. *Appl. Therm. Eng.* **2020**, *174*, 115204. [[CrossRef](#)]
11. Wang, X.; Dong, J.; Zhang, G.; Fu, Q.; Li, H.; Han, Y.; Tu, J. The primary pseudo-shock pattern of steam ejector and its influence on pumping efficiency based on CFD approach. *Energy* **2019**, *167*, 224–234. [[CrossRef](#)]
12. Varga, S.; Oliveira, A.C.; Diaconu, B. Numerical assessment of steam ejector efficiencies using CFD. *Int. J. Refrig.* **2009**, *32*, 1203–1211. [[CrossRef](#)]
13. Pianthong, K.; Seehanam, W.; Behnia, M.; Sriveerakul, T.; Aphornratana, S. Investigation and improvement of ejector refrigeration system using computational fluid dynamics technique. *Energy Convers. Manag.* **2007**, *48*, 2556–2564. [[CrossRef](#)]
14. Li, H.; Wang, X.; Ning, J.; Zhang, P.; Huang, H.; Tu, J. Numerical investigation of the nozzle expansion state and its effect on the performance of the steam ejector based on ideal gas model. *Appl. Therm. Eng.* **2021**, *199*, 117509. [[CrossRef](#)]
15. Wang, X.; Lei, H.; Dong, J.; Tu, J. The spontaneously condensing phenomena in a steam-jet pump and its influence on the numerical simulation accuracy. *Int. J. Heat Mass Transf.* **2012**, *55*, 4682–4687. [[CrossRef](#)]
16. Sharifi, N.; Boroomand, M.; Sharifi, M. Numerical assessment of steam nucleation on thermodynamic performance of steam ejectors. *Appl. Therm. Eng.* **2013**, *52*, 449–459. [[CrossRef](#)]
17. Zheng, H.T.; Cai, L.; Li, Y.J.; Li, Z.M. Computational fluid dynamics simulation of the supersonic steam ejector. Part 1: Comparative study of different equations of state. *Proc. Inst. Mech. Eng. Part C J. Mech. Eng. Sci.* **2012**, *226*, 709–714. [[CrossRef](#)]
18. Foroozesh, F.; Khoshnevis, A.B.; Lakzian, E. Improvement of the wet steam ejector performance in a refrigeration cycle via changing the ejector geometry by a novel EEC (Entropy generation, Entrainment ratio, and Coefficient of performance) method. *Int. J. Refrig.* **2020**, *110*, 248–261. [[CrossRef](#)]
19. Ariafar, K.; Buttsworth, D.; Al-Doori, G.; Malpress, R. Effect of mixing on the performance of wet steam ejectors. *Energy* **2015**, *93*, 2030–2041. [[CrossRef](#)]
20. Lei, Y.; Li, S.; Lu, J.; Xu, Y.; Yong, Y.; Xing, D. Numerical Analysis of Steam Ejector Performance with Non-Equilibrium Condensation for Refrigeration Applications. *Buildings* **2023**, *13*, 1672. [[CrossRef](#)]
21. Wang, C.; Wang, L. Investigation of Fluid Characteristic and Performance of an Ejector by a Wet Steam Model. *Entropy* **2023**, *25*, 85. [[CrossRef](#)] [[PubMed](#)]
22. Zhang, G.; Dykas, S.; Yang, S.; Zhang, X.; Li, H.; Wang, J. Optimization of the primary nozzle based on a modified condensation model in a steam ejector. *Appl. Therm. Eng.* **2020**, *171*, 115090. [[CrossRef](#)]
23. Zhang, G.; Wang, X.; Pourranjbar, D.; Dykas, S.; Li, H.; Chen, J. The comprehensive analysis of the relationship between the latent heat, entrainment ratio, and ejector performance under different superheating degree conditions considering the non-equilibrium condensation. *Appl. Therm. Eng.* **2022**, *200*, 117701. [[CrossRef](#)]
24. Mazzelli, F.; Giacomelli, F.; Milazzo, A. CFD modeling of condensing steam ejectors: Comparison with an experimental test-case. *Int. J. Therm. Sci.* **2018**, *127*, 7–18. [[CrossRef](#)]
25. Yang, Y.; Walther, J.H.; Yan, Y.; Wen, C. CFD modeling of condensation process of water vapor in supersonic flows. *Appl. Therm. Eng.* **2017**, *115*, 1357–1362. [[CrossRef](#)]
26. Kantrowitz, A. Nucleation in Very Rapid Vapor Expansions. *J. Chem. Phys.* **1951**, *19*, 1097–1100. [[CrossRef](#)]
27. Simpson, D.A.; White, A.J. Viscous and unsteady flow calculations of condensing steam in nozzles. *Int. J. Heat Fluid Flow* **2005**, *26*, 71–79. [[CrossRef](#)]
28. Zhang, G.; Zhang, X.; Wang, F.; Wang, D.; Jin, Z.; Zhou, Z. Design and optimization of novel dehumidification strategies based on modified nucleation model in three-dimensional cascade. *Energy* **2019**, *187*, 115982. [[CrossRef](#)]
29. Young, J.B. Spontaneous condensation of steam in supersonic nozzles. *PCH Physicochem. Hydrodyn.* **1982**, *3*, 57–82.
30. Young, B.J. An Equation of State for Steam for Turbomachinery and Other Flow Calculations. *J. Eng. Gas Turbines Power* **1988**, *110*, 1–7. [[CrossRef](#)]
31. Yang, Y.; Zhu, X.; Yan, Y.; Ding, H.; Wen, C. Performance of supersonic steam ejectors considering the nonequilibrium condensation phenomenon for efficient energy utilization. *Appl. Energy* **2019**, *242*, 157–167. [[CrossRef](#)]
32. Moore, M.J.; Walters, P.T.; Crane, R.I.; Davidson, B.J. Predicting the fog-drop size in wet-steam turbines. In *Wet Steam 4 Conference*; Institute of Mechanical Engineers (UK), University of Warwick: Coventry, UK, 1973.
33. Aldoori, G. Investigation of Refrigeration System Steam Ejector Performance through Experiments and Computational Simulations. Ph.D. Thesis, University of Southern Queensland, Toowoomba, QLD, Australia, 2013.
34. Cinar, G.; Yilbas, B.S.; Sunar, M. Study into nucleation of steam during expansion through a nozzle. *Int. J. Multiph. Flow* **1997**, *23*, 1171–1188. [[CrossRef](#)]

Disclaimer/Publisher’s Note: The statements, opinions and data contained in all publications are solely those of the individual author(s) and contributor(s) and not of MDPI and/or the editor(s). MDPI and/or the editor(s) disclaim responsibility for any injury to people or property resulting from any ideas, methods, instructions or products referred to in the content.